Cross Interference Minimization and Simultaneous Wireless Power Transfer to Multiple Frequency Loads Using Frequency Bifurcation Approach

Narayanamoorthi R., *Member, IEEE*, Vimala Juliet A., and Bharatiraja Chokkalingam, *Member, IEEE*

***Abstract*—Simultaneous power distribution to multiple loads using a single source in the wireless power transfer (WPT) system is a challenging issue due to cross-coupling between the load coils, which reduces the power transfer efficiency. In a resonant WPT system, when two or more coils operated under over coupled condition, the original operating resonant frequency gets bifurcated, and thereby reduction in the power transfer efficiency. Different techniques are investigated in the literature to mitigate the frequency bifurcation phenomena in the resonant WPT system. However, the utilization of frequency bifurcation approach for the simultaneous power transfer to multiple loads is not addressed. This paper proposes a simultaneous power transfer approach using frequency bifurcation for the multiple load system designed with different operating frequency. Mathematical, simulation, and experimental studies performed for dual, triple, and four coil WPT systems with multiple loads. In addition, an automatic power flow control method is implemented to estimate the load current from the source, which helps to select a new set of load coils to be charged. The experimental results confirm the proposed power transfer, helps to attain higher power transfer efficiency of 39.34%, 49.31%, 68.22% and cross interference of −31.2 dBV, −36.2 dBV, −41.2 dBV for dual, triple, and four coil WPT system, respectively.**

***Index Terms*—Frequency bifurcation, multiple receivers, selective wireless power transfer (WPT), simultaneous power transfer, wireless power.**

I. Introduction

MAGNETIC resonance wireless power transfer (WPT) is now extensively investigated as an alternative method to charge different electric and electronic devices [1]–[4]. In some of the low power applications such as distributed implants, swarm robots, and mobile phones may need to transfer power to more than one receiver's (Rx). In such applications, the simultaneous power transfer to multiple Rx's with a single transmitter (Tx) will be a preferable choice by the end user. One

Manuscript received December 30, 2018; accepted February 1, 2019. Date of publication February 11, 2019; date of current version August 29, 2019. Recommended for publication by Associate Editor C. K. Tse. *(Corresponding author: Narayanamoorthi R.)*

N. R. and B. Chokkalingam are with the Department of Electrical and Electronics Engineering, SRM Institute of Science and Technology, Chennai 603203, India (e-mail:

parallel coils is indirectly proportional to the center center separation between the coil [21]. For mid-range applications, the conventional dual coil WPT system has replaced with a triple and four coil WPT system in each Tx–Rx pairs to increase the power transfer efficiency [22]–[24]. However, when the coils are over coupled (OC), frequency bifurcation occurs in the Rx power that deviates the original operating resonant frequency and thereby reduction in the power transfer efficiency [25]. The bifurcated frequency pattern will be changing depending on the number of coils used in the Tx to Rx link [26]–[28]. Different techniques like impedance matching and Tx frequency tuning are investigated to mitigate the frequency bifurcation phenomena [29]–[31]. However, there is no much work is done to use the frequency s bifurcation phenomena for the power transmission in multiple Rx WPT system.

Based on the abovementioned discussion, it is observed that the simultaneous charging, cross-coupling elimination, and flexibility to design Rx's with different resonant frequencies are the basic needs to be addressed in multiple Rx system. To overcome the aforementioned limitations, this paper presents the following novel contributions in multiple Rx WPT system.

1) The frequency bifurcation presented in the resonant WPT system is utilized to simultaneously charge multiple loads without much cross interference between the adjacent load coils. The proposed method does not require any tuning circuit at the Tx or Rx side.
2) Initially, the frequency bifurcation phenomena in dual, triple, and four coil WPT systems are analyzed to determine the mathematical expression for the bifurcated frequency at a different coupling point.
3) The simultaneous power transfer to multiple loads is examined by using dual, triple, and four coils at the transmission link. The mathematical derivations, circuit simulation, and finite element method (FEM) analysis are performed for the proposed WPT system to determine the power transfer ratio.
4) An automatic power flow control approach has been developed to simultaneously charge a different group of loads by changing the coupling at the Tx coils.

The experimental investigations are carried out in both CC and OC modes to validate the proposed multiple Rx WPT system. From the simulation and experimental results, it has observed that by designing the load coils frequency as same as Rx split frequencies, the power flow becomes simultaneous and independent of cross interference.

II. Frequency Bifurcation in Dual, Triple, and Four Coil Systems

The frequency bifurcation pattern in dual, triple, and four coil WPT system under OC mode are different. In order to determine the bifurcation frequency, the analysis is carried out by considering all the coils have the same dimensions with the circuit parameters of $R = 50.5\ \Omega$, $L = 25.3\ \mu$H, $C = 10$ pF, and $f = 10$ MHz. The drive coil, Tx coil, Rx1, Rx2, and load coil parameters are denoted with subscripts of D, T, R1, R2, and L, respectively. The self-impedance, mutual impedance,

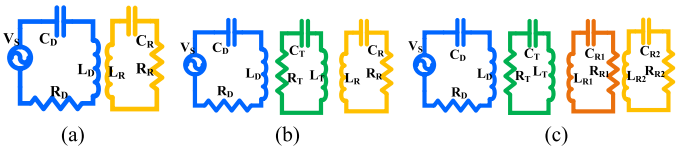

Fig. 1. WPT equivalent circuit. (a) Dual coil MRWPT. (b) Triple coil MRWPT. (c) Four coil MRWPT.

coupling coefficient, and critical coupling of the coil is represented as $Z_{ii} = R_i + j(\omega L_i - \frac{1}{\omega C_i})$; $Z_{ij} = j\omega M_{ij}; i, j = D,\ T,\ R(R1),\ R2; k_{ij} = \frac{M_{ij}}{\sqrt{L_i L_j}}$ and $k_c = \frac{1}{\sqrt{Q_i Q_j}}$. The dual coil WPT system consists of a drive coil and an Rx coil as shown in Fig. 1(a).

By applying KVL to the circuit in Fig. 1(a)

$$\begin{bmatrix} V_s \\ 0 \end{bmatrix} = \begin{bmatrix} Z_D & j\omega M_{DR} \\ j\omega M_{RD} & Z_R \end{bmatrix} \begin{bmatrix} I_D \\ I_R \end{bmatrix}. \tag{1}$$

Rearranging (1) with the inductor ratio of $T = \sqrt{\frac{L_i}{L_j}}; i,\ j = D,\ T,\ R1,\ R2$ and the transformed impedance $Z'_i = \frac{R_i}{j\omega L_i} + (1 - \frac{\omega_0^2}{\omega^2}); i = D,\ T,\ R1,\ R2$, where $\omega_0 = \frac{1}{\sqrt{L_i C_i}}$

$$\begin{bmatrix} Z'_D & Tk_{DR} \\ T^{-1}k_{RD} & Z'_R \end{bmatrix} \begin{bmatrix} I_D \\ I_R \end{bmatrix} = \frac{1}{j\omega L_D} \begin{bmatrix} V_s \\ 0 \end{bmatrix}. \tag{2}$$

In magnetic resonance WPT system, under the CC and OC modes of operation with high-quality factor (Q) coil, the magnitude of $j\omega L \gg R$ [27]. It implies $\frac{R}{\omega L}$ and $\frac{V_s}{\omega L}$ are negligible, and the transformed self-impedance of the coil tends to one, i.e., $Z'_{ii} = 1$

$$\begin{bmatrix} 1 & Tk_{DR} \\ T^{-1}k_{RD} & 1 \end{bmatrix} \begin{bmatrix} I_D \\ I_L \end{bmatrix} = \begin{bmatrix} 0 \\ 0 \end{bmatrix}. \tag{3}$$

Solving the impedance matrix in (3), the bifurcated frequencies of the Rx coil are

$$\omega_1 = \frac{\omega_0}{\sqrt{1 + k_{DR}}};\ \omega_2 = \frac{\omega_0}{\sqrt{1 - k_{DR}}}. \tag{4}$$

The coupling coefficient concerning to coil separation (d_{DR}) is expressed as

$$k_{DR} = \frac{\omega_0}{\left[1 + \frac{2^{1.5} d_{DR}^2}{r_D r_R}\right]^{\frac{3}{2}}}. \tag{5}$$

From (1) and (2) the PTR of the dual coil system will be

$$P_{DR} = \frac{\omega^2 k_{DR}^2 R_D R_R L_D L_R}{\left(Z_D Z_R + \omega^2 k_{DR}^2 L_D L_R\right)^2}. \tag{6}$$

Analytical simulation results of the dual coil system for different coupling coefficients are shown in Fig. 2(a). When the coupling coefficient (k_{DR}) between the coil is kept less than 0.05, there will not be any deviation in the original resonant frequency. As k_{DR} is increased above 0.05, the peak power in the receiver occurs at two different frequencies.

The triple coil WPT system consists of the drive coil, Tx coil, and Rx coil as shown in Fig. 1(b). Since the drive and Rx coils coupled through Tx coil, the coupling between the drive and Rx

coils are weak as compared with the coupling between drive- Tx and Tx- Rx, hence k_{DR}, k_{RD} can be negligible. By applying KVL to the triple coil circuit

$$\begin{bmatrix} Z'_D & Tk_{DT} & 0 \\ T^{-1}k_{TD} & Z'_T & Tk_{TR} \\ 0 & T^{-1}Z_{RT} & Z'_R \end{bmatrix} \begin{bmatrix} I_D \\ I_T \\ I_R \end{bmatrix} = \begin{bmatrix} 0 \\ 0 \\ 0 \end{bmatrix}. \quad (7)$$

Solving the 3×3 impedance matrix (7), the bifurcated frequency and power transfer ratio of the system is

$$\omega_1 = \omega_0; \quad \omega_2 = \frac{\omega_0}{1 - \sqrt{k_{DT}^2 + k_{TR}^2}};$$

$$\omega_3 = \frac{\omega_0}{1 + \sqrt{k_{DT}^2 + k_{TR}^2}}. \quad (8)$$

The coupling coefficient concerning to drive- Tx and Tx- Rx coil separation is given as

$$k_{DT} = \frac{\omega_0}{\left[1 + \frac{2^{1.5} d_{DT}^2}{r_D r_T}\right]^{\frac{3}{2}}}; \; k_{TR} = \frac{\omega_0}{\left[1 + \frac{2^{1.5} d_{TR}^2}{r_T r_R}\right]^{\frac{3}{2}}}. \quad (9)$$

The power transfer ratio of triple coil WPT with respect to coupling and inductance given as

$$P_{DR} = \frac{4\omega^4 k_{DT}^2 k_{TR}^2 L_T^2 R_D R_R L_D L_R}{\left[Z_D Z_T Z_R + \omega^2 \left(k_{DT}^2 L_D L_T Z_R + k_{TR}^2 L_T L_R Z_R\right)\right]^2}. \quad (10)$$

The analytical simulation results of a triple coil system are shown in Fig. 2(b). It is observed that three frequency components are present in the OC region and the peak-valley of the Rx power occurs at three different frequencies including the original resonant frequency (10 MHz).

Four coil WPT system has a drive coil, Tx coil, Rx1 coil, and Rx2 coil as shown in Fig. 1(c). The coupling between the drive- Rx1, drive- Rx2, and Tx- Rx2 are small, this makes k_{DR2}, k_{R2D}, k_{TR2}, k_{R2T}, k_{DR1}, and k_{R1D} negligible and the voltage current relationship of four coil system is (11) shown at the bottom of this page.

The bifurcated frequency of the four coil system is in (12) shown at the bottom of this page.

The analytical simulation results of PTR for the four coil MRWPT system are shown in Fig. 2(c). Four peak-valley occurs at a different frequency in the Rx2 power under OC mode. Based on the abovementioned analysis, it is observed that with the increase in the number of coils in the WPT system, the number of bifurcated frequency components also increases under OC mode. Also, in even number of coil system the original resonant frequency is not present under OC mode, whereas in an odd number of coil system original resonant frequency is present along with bifurcated frequency components. The magnitude of received power at each bifurcated frequency is higher in OC mode as compared to CC mode. The PTR for dual, triple, and four coil systems for different coupling coefficients are given in Table I.

TABLE I
FREQUENCY AND PTR FOR DIFFERENT COUPLING

(k)	Dual coil MRWPT		Triple coil MRWPT			Four coil MRWPT			
	f_1 (MHz) /PTR	f_2 (MHz) / PTR	f_1 (MHz) /PTR	f_2 (MHz) /PTR	f_3 (MHz) / PTR	f_1 (MHz) / PTR	f_2 (MHz) / PTR	f_3 (MHz) /PTR	f_4 (MHz) /PTR
0.05	10 0.48	-	8.4 0.173	10 0.244	12.9 0.230	8.5 0.979	12.7 0.981	12.9 0.784	13.2 0.953
0.20	9.1 0.49	11.2 0.498	8.3 0.726	10 0.791	13.4 0.742	8.1 0.642	8.7 0.911	12.1 0.963	14.3 0.964
0.35	8.6 0.49	12.4 0.49	8.1 0.953	10 0.981	14.60 0.969	7.9 0.869	8.9 0.980	11.6 0.949	16.1 0.898
0.50	8.2 0.496	14.1 0.498	7.8 0.909	10 0.965	16.7 0.952	7.6 0.591	9.1 0.91	11.3 0.962	19.0 0.927
0.65	7.8 0.498	16.90 0.499	7.5 0.663	10 0.883	20.5 0.863	7.4 0.565	9.2 0.969	11.0 0.985	25 0.927

III. SIMULTANEOUS SELECTIVE WPT SYSTEM

For the simultaneous charge of multiple devices which are located close to each other, the resonant frequency of each should be different to minimize cross coupling, and the source needs to transfer the power at multiple resonant frequencies. The proposed method operates on frequency bifurcation based power division technique for multiple loads which are designed with the different resonant frequency. It can be achieved by designing the load coil resonant frequency as same as the bifurcated frequency in the Rx coils and operating the Tx and Rx in OC mode. When the Tx and Rx coils are operated under CC mode, only a single load which is designed with the same frequency as of drive coil can get maximum power. However, under OC

$$\begin{bmatrix} Z'_D & TZ_{DT} & 0 & 0 \\ T^{-1}Z_{TD} & Z'_T & TZ_{TR1} & 0 \\ 0 & T^{-1}Z_{R1T} & Z'_{R1} & TZ_{R1R2} \\ 0 & 0 & T^{-1}Z_{R2R1} & Z'_{R2} \end{bmatrix} \begin{bmatrix} I_D \\ I_T \\ I_{R1} \\ I_{R2} \end{bmatrix} = \begin{bmatrix} 0 \\ 0 \\ 0 \\ 0 \end{bmatrix} \quad (11)$$

$$\left.\begin{aligned} \omega_{1,2} &= \frac{\sqrt{2}\omega_0}{\sqrt{2 + \left(\sqrt{2}\left\{k_{DT}^2 + k_{TR1}^2 + k_{R1R2}^2 \pm \left[\left(k_{DT}^2 + k_{TR1}^2\right)^2 + 2k_{R1R2}^2\left(k_{TR1}^2 - k_{DT}^2\right) + k_{R1R2}^4\right]^{\frac{1}{2}}\right\}^{1/2}\right)}} \\ \omega_{3,4} &= \frac{\sqrt{2}\omega_0}{\sqrt{2 - \left(\sqrt{2}\left\{k_{DT}^2 + k_{TR1}^2 + k_{R1R2}^2 \pm \left[\left(k_{DT}^2 + k_{TR1}^2\right)^2 + 2k_{R1R2}^2\left(k_{TR1}^2 - k_{DT}^2\right) + k_{R1R2}^4\right]^{\frac{1}{2}}\right\}^{\frac{1}{2}}\right)}} \end{aligned}\right\} \quad (12)$$

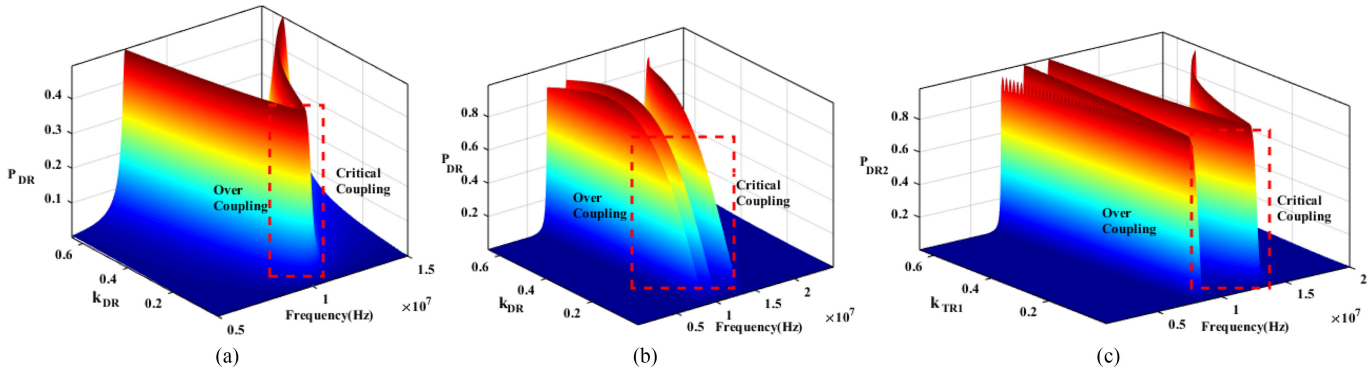

Fig. 2. Power transfer ratio of WPT. (a) Dual coil. (b) Triple coil. (c) Four coil.

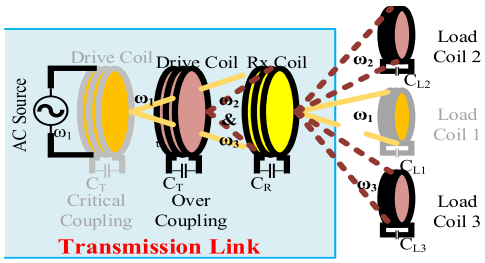

Fig. 3. Dual coil SSWPT.

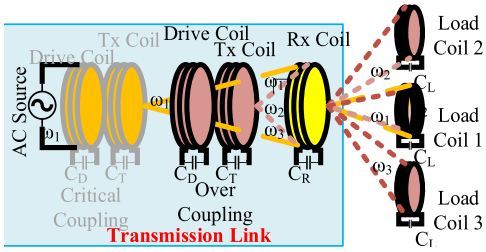

Fig. 4. Triple coil SSWPT.

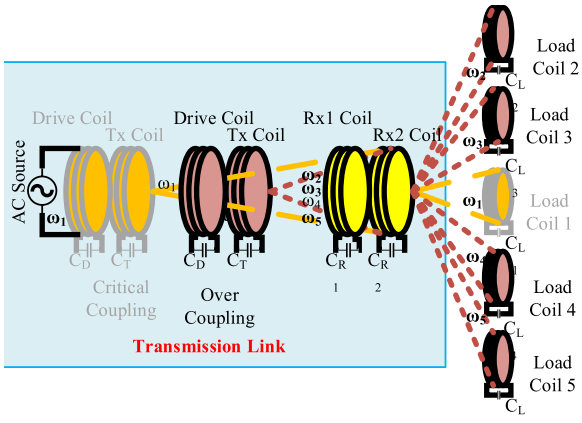

Fig. 5. Four coil SSWPT.

mode, the dual, triple, and four coil systems can simultaneously transfer power to two, three, and four loads, respectively, which are designed with the different resonant frequency. Figs. 3–5 illustrate the schematic model of the proposed simultaneous selective wireless power transfer system (SSWPT) with dual, triple, and four coil transmission link. The dimmed portion represent the CC mode and bright portion of the coil represent the OC mode. Whenever the coupling between coil changes, the bifurcated frequency values will be changing and to track the designed load frequency, proper selection of distance between the Tx and Rx and coupling coefficients are required. The selection of load coils resonant frequency from the bifurcated frequency of Rx coil is done with minimum bandwidth separation between different loads to curtail the cross coupling effect

$$\omega_1 = \frac{1}{\sqrt{L_D C_D}}; \quad \omega_2 = \frac{1}{\sqrt{L_{L2} C_{L2}}};$$
$$\omega_3 = \frac{1}{\sqrt{L_{L3} C_{L3}}}; \quad \omega_4 = \frac{1}{\sqrt{L_{L4} C_{L4}}}. \tag{13}$$

The distance between the Rx and load coils is maintained at a CC mode or loosely coupling mode such that there will not be any further deviation in the resonant frequency between the Rx and loads. The received power at the load depends on the loss in each resonator coil and leakage flux at each stage. Table III gives the calculated values of bifurcated frequencies, coupling coefficient, and circuit design parameters of the system. The load coils are designed by first determining the bifurcated frequency, inductance values and then calculating the capacitance from (13). The inductance values are calculated using wheeler's formula by considering the design constrains, and the same values are used for circuit simulation [32]. The complete design procedure of the proposed WPT system illustrated in Fig. 6.

A. Power Transfer Ratio of SSWPT System

The power transfer ratio of the proposed SSWPT system is derived by considering the permissible assumption that the cross coupling between different load coils are negligible due to different self-resonant frequency.

Case 1: Dual coil SSWPT system

The voltage and current relationship of the dual coil SSWPT system can be derived by applying KVL to the circuit shown in Fig. 5. Since the load coils are designed with different resonant frequency and coupled through Rx coil, the cross coupling between the load coils can be neglected, i.e., k_{L1L2}, k_{L1L3}, k_{L2L3}, k_{DL}, k_{LD}, k_{L2L1}, k_{L3L1}, and k_{L3L2} are assumed to be zero. The

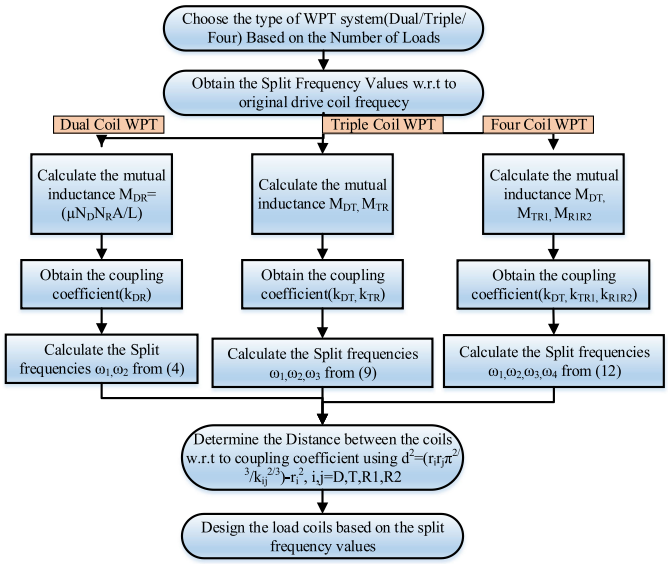

Fig. 6. Flowchart of proposed system design.

current in each resonant coil can be estimated as

$$\begin{bmatrix} I_D \\ I_R \\ .. \\ ..I_{L3} \end{bmatrix} = \begin{bmatrix} Z_D & T_{DR}k_{DR} & .. & 0 \\ T_{DR}^{-1}k_{RD} & Z_R & .. & T_{RL3}k_{RL3} \\ 0 & T_{RL1}^{-1}k_{L1R} & .. & 0 \\ 0 & T_{RL3}^{-1}k_{L3R} & .. & Z_{L3} \end{bmatrix}^{-1} \times \begin{bmatrix} V_s \\ 0 \\ 0 \\ 0 \end{bmatrix}. \tag{14}$$

The drive and load coil currents are

$$I_D = \frac{V_s\left(\frac{k_{RL1}^2}{Z_{L1}} + \frac{k_{RL2}^2}{Z_{L2}} + \frac{k_{RL3}^2}{Z_{L3}} - Z_R\right)}{A} \tag{15}$$

$$I_{Li} = \frac{-V_s k_{DR} k_{RLi}}{T_{DR} T_{RLi} Z_{Li} A}; i = 1,\ 2,\ 3 \tag{16}$$

where $A = [k_{DR}^2 + Z_D(\frac{k_{RL1}^2}{Z_{L1}} + \frac{k_{RL2}^2}{Z_{L2}} + \frac{k_{RL3}^2}{Z_{L3}} - Z_R)]$.

From (15) and (16), the power transfer ratio of each load is

$$\frac{P_{Li}}{P_D} = \frac{k_{DR}^2 k_{RLi}^2\ R_{Li}}{\left[T_{DR}T_{RLi}Z_{Li}\left(\frac{k_{RLi}^2}{Z_{L1}} + \frac{k_{RL2}^2}{Z_{L2}} + \frac{k_{RL3}^2}{Z_{L3}} - Z_R\right)\right]^2 R_D}; \quad i = 1,\ .3. \tag{17}$$

For the fixed distance and CC mode between the Rx and loads, the PTR of each load from the drive coil depends on the coupling between the drive - Rx and self-resonant frequency of the load coil. The load impedance $Z_{L1},\ Z_{L2},\ Z_{L3}$ values are calculated at the self-resonant frequency of ω_1, ω_2, and ω_3, respectively.

Case 2: Triple Coil SSWPT

For the triple coil SSWPT system shown in Fig. 6, the voltage current relation can be obtained by neglecting the cross coupling, i.e., $k_{L1L2}, k_{L1L3}, k_{L2L3}, k_{DL}, k_{LD}, k_{L2L1}, k_{L3L1}, k_{L3L2}, k_{TL}$, k_{LT}, and k_{DR} are assumed to be zero

$$\begin{bmatrix} I_D \\ .. \\ I_R \\ .. \\ I_{L3} \end{bmatrix} = \begin{bmatrix} Z_D & .. & 0 & .. & 0 \\ T_{DT}^{-1}k_{TD} & .. & T_{TR}k_{TR} & .. & 0 \\ 0 & .. & Z_R & .. & T_{RL3}k_{RL3} \\ .. & .. & T_{RL2}^{-1}k_{L2R} & .. & 0 \\ 0 & .. & T_{RL3}^{-1}k_{L3R} & .. & Z_{L3} \end{bmatrix}^{-1} \times \begin{bmatrix} V_s \\ 0 \\ 0 \\ 0 \\ 0 \end{bmatrix}. \tag{18}$$

The drive and load currents are given as

$$I_D = \frac{V_s B}{k_{DT}^2\left(Z_R - \frac{k_{RL1}^2}{Z_{L1}} - \frac{k_{RL2}^2}{Z_{L2}} - \frac{k_{RL3}^2}{Z_{L3}}\right) + Z_D B} \tag{19}$$

where $B = Z_D(\frac{k_{RL1}^2}{Z_{L1}} + \frac{k_{RL2}^2}{Z_{L2}} + \frac{k_{RL3}^2}{Z_{L3}} + \frac{k_{TR}^2}{Z_T} - Z_R)$ and the power transfer ratio for each load is calculated from (19)–(20), eq. (20) shown at the bottom of this page.

$$\frac{P_{Li}}{P_D} = \frac{k_{RLi}^2 k_{TR}^2 R_{Li}}{Z_{Li}^2 T_{DT}^2 T_{RLi}^2 T_{TR}^2 B^2 R_D}; i = 1,\ 2,\ 3. \tag{21}$$

Case 3: Four Coil SSWPT System

Similarly, for the four coil SSWPT system the voltage current relationship is governed by applying KVL to Fig. 6 and neglecting the cross coupling i.e., $k_{L1L2}, k_{L1L3}, k_{L1L4}, k_{L1L5}$, $k_{L2L3}, k_{L2L4}, k_{L2L5}, k_{L3L4}, k_{L3L5}, k_{DL}, k_{LD}, k_{LR1}, k_{R1L}$, $k_{DR2}, k_{TL}, k_{LT}, k_{DR1}$ are assumed to be zero.

$$\begin{bmatrix} I_D \\ .. \\ I_{R2} \\ .. \\ I_{L5} \end{bmatrix} = \begin{bmatrix} Z_D & .. & 0 & 0 \\ T_{DT}^{-1}k_{TD} & .. & 0 & 0 \\ 0 & .. & Z_{R2} & T_{R2L5}k_{R2L5} \\ 0 & .. & .. & .. \\ 0 & .. & T_{R2L5}^{-1}k_{L5R2} & Z_{L5} \end{bmatrix}^{-1} \times \begin{bmatrix} V_s \\ 0 \\ 0 \\ 0 \\ 0 \end{bmatrix}. \tag{22}$$

$$I_{Li} = \frac{V_s k_{DT} k_{RLi} k_{TR}}{Z_{Li} T_{DT} T_{RLi} T_{TR}\left[k_{DT}^2\left(Z_R - \frac{k_{RL1}^2}{Z_{L1}} - \frac{k_{RL2}^2}{Z_{L2}} - \frac{k_{RL3}^2}{Z_{L3}}\right) + Z_D B\right]} \tag{20}$$

TABLE II
SSWPT SYSTEM PARAMETERS

Parameters	2 coil	3 coil	4 coil	f (MHz)
L_D / L_T / L_{R1} / L_{R2} (μH)	25.3	25.3	25.3	10
C_D / C_T / C_{R1}/ C_{R2} (pF)	10	10	10	
R_D/ R_T/ R_{R1}/ R_{R2} (Ω)	50.5	50.5	50.5	
N_D/ N_T/ N_{R1}/ N_{R2}	5	5	5	
Q_D/ Q_T/ Q_{R1}/ Q_{R2}	172	172	172	
L_{L1} (μH)	25.3	25.3	25.3	f_{2coil} =10 f_{3coil} =10 f_{4coil} =10
C_{L1} (pF)	10	10	10	
R_{L1} (Ω)	0.5	0.5	0.5	
N_{L1}	5	5	5	
Q_{L1}	172	172	172	
L_{L2} (μH)	34.1	38.5	40.5	f_{2coil} = 8.6 f_{3coil} = 8.1 f_{4coil} = 7.9
C_{L2} (pF)	10	10	10	
R_{L2} (Ω)	0.5	0.5	0.5	
N_{L2}	7	8	8	
Q_{L2}	245	231	223	
L_{L3} (μH)	16.49	11.9	32	f_{2coil} =12.4 f_{3coil} =14.6 f_{4coil} =8.9
C_{L3} (pF)	10	10	10	
R_{L3} (Ω)	0.5	0.5	0.5	
N_{L3}	3	3	6	
Q_{L3}	282	291	166	
L_{L4} (μH)	-	-	18.5	f_{4coil} =11.7
C_{L4} (pF)	10	10	10	
R_{L4} (Ω)	0.5	0.5	0.5	
N_{L4}	-	-	4	
Q_{L4}	-	-	212	
L_{L5} (μH)	-	-	9.7	f_{4coil} =16.1
C_{L5} (pF)	10	10	10	
R_{L5} (Ω)	0.5	0.5	0.5	
N_{L5}	-	-	2	
Q_{L5}	-	-	298	

TABLE III
PTR OF DUAL COIL SSWPT SYSTEM

$f(MHz)$	Mode	$\frac{P_{Rx}}{P_D}$	$\frac{P_{L1}}{P_D}$	$\frac{P_{L2}}{P_D}$	$\frac{P_{L3}}{P_D}$
10	**CC**	0.69(0.71)	0.59(0.6)	0.08(0.06)	0.01(0.01)
	OC	0.18(0.17)	0.01(0.01)	0.01(0.01)	0.04(0.03)
8.6	**CC**	0.001(0.001)	0.001(0.001)	0.11(0.001)	0.02(0.01)
	OC	0.59(0.60)	0.02(0.01)	0.58(0.59)	0.01(.001)
12.4	**CC**	0.001(0.001)	0.001(0.001)	0.001(.001)	0.04(0.03)
	OC	0.60(0.61)	0.02(0.01)	0.04(0.02)	0.58(0.60)

() denotes analytical result

The power transfer ratio of each load coil to the drive coil is

$$\frac{P_{Li}}{P_D} = \frac{k_{DT}^2 k_{TR1}^2 k_{R1R2}^2 k_{R2Li}^2 R_{Li}}{Z_{Li}^2 T_{DT}^2 T_{TR1}^2 T_{R1R2}^2 T_{R2Li}^2 E^2 R_D}; i = 1..5 \quad (23)$$

where $E = Z_D(\frac{k_{R2L1}^2}{Z_{L1}} + \frac{k_{R2L2}^2}{Z_{L2}} + \frac{k_{R2L3}^2}{Z_{L3}} + \frac{k_{R2L4}^2}{Z_{L4}} + \frac{k_{R2L5}^2}{Z_{L5}} + \frac{k_{R1R2}^2}{Z_{R1}} - Z_{R2})$

The load impedance Z_{L1}, Z_{L2}, Z_{L3}, Z_{L4}, and Z_{L5} values are calculated with the self-resonant frequency of ω_1, ω_2, ω_3, ω_4, and ω_5, respectively.

In all the cases, the power transfer to the load depends on the Rx coil power and the coupling between the load and Rx. The overall efficiency of the system depends on the power loss at each coil and PTR between the resonators. The analytical calculations of load PTR are performed for each case with the specifications given in Table II and the results are compared with the simulation results as shown in Table III-V.

TABLE IV
PTR OF TRIPLE COIL SSWPT SYSTEM

$f(MHz)$	Mode	$\frac{P_{Rx}}{P_D}$	$\frac{P_{L1}}{P_D}$	$\frac{P_{L2}}{P_D}$	$\frac{P_{L3}}{P_D}$
10	**CC**	0.87(0.88)	0.68(0.68)	0.001(.001)	0.001(.001)
	OC	0.69(0.71)	0.59(0.59)	0.08(0.06)	0.04(0.03)
8.1	**CC**	0.001(.001)	0.001(.001)	0.1(0.06)	0.001(.001)
	OC	0.48(0.49)	0.01(0.01)	0.48(0.49)	0.001(.001)
14.6	**CC**	.001(.001)	.001(.001)	.001(0.001)	0.08(0.03)
	OC	0.51(0.51)	0.02(0.01)	0.02(0.02)	0.51(0.53)

() denotes analytical result

TABLE V
PTR OF FOUR COIL SSWPT SYSTEM

f $(MHz$	Mode	$\frac{P_{Rx}}{P_D}$	$\frac{P_{L1}}{P_D}$	$\frac{P_{L2}}{P_D}$	$\frac{P_{L3}}{P_D}$	$\frac{P_{L4}}{P_D}$	$\frac{P_{L5}}{P_D}$
10	**CC**	0.92 (0.94)	0.78 (0.79)	0.01 (0.01)	0.01 (0.01)	0.02 (0.001)	0.01 (.006)
	OC	0.16 (0.1)	0.02 (0.01)	0.01 (0.01)	0.001 (0.001)	0.04 (0.03)	0.001 (.001)
7.9	**CC**	0.001 (.001)	.001 (.001)	0.1 (0.08)	0.01 (0.01)	.001 (0.001)	.001 (.001)
	OC	0.49 (0.51)	0.01 (0.01)	0.49 (0.50)	0.1 (0.07)	0.04 (0.04)	.001 (.001)
8.9	**CC**	0.001 (.001)	.001 (.001)	0.01 (0.01)	0.1 (0.07)	0.001 (.001)	.001 (.001)
	OC	0.60 (0.61)	0.01 (0.01)	0.08 (0.06)	0.59 (0.60)	0.02 (0.01)	0.001 (.001)
11.7	**CC**	0.001 (.001)	.001 (.001)	0.01 (0.01)	.001 (.001)	0.14 (0.01)	0.001 (.001)
	OC	0.62 (0.62)	0.01 (0.01)	0.02 (0.01)	0.08 (0.07)	0.58 (0.61)	0.06 (.051)
16.1	**CC**	0.001 (.001)	0.001 (.001)	0.01 (0.01)	0.001 (.001)	0.001 (.001)	0.001 (.001)
	OC	0.59 (0.61)	0.001 (.001)	0.02 (0.01)	0.02 (0.01)	0.08 (0.06)	0.59 (0.60)

() denotes analytical result

B. Simulation Verification of SSWPT System

The proposed SSWPT model is simulated in time and frequency domain using advanced design system software tool to determine the PTR and voltage received at each load. Fig. 7 shows the magnitude of PTR between drive- Rx and drive- load coils under CC and OC modes for dual, triple, and four coil SSWPT systems. It is observed that under CC mode, the load 1 which is designed with 10 MHz resonant frequency is receiving maximum PTR of 0.59, 0.69, and 0.78 in dual, triple, and four coil SSWPT system, respectively. The PTR of load 2 to load 5 are less than 0.15 under the CC mode. When the coupling coefficient between the Tx and Rx is increased to 0.35, the load 2 and load 3, which are designed with 8.6 MHz and 12.4 MHz are receiving maximum power in dual coil SSWPT system. In case of triple coil system, the PTR of all the three loads are maximum at the bifurcated frequency and for the four coil system, except load 1 the remaining four loads are receiving the maximum power at the designed self-resonant frequency.

The effect of cross coupling from the other Rx's are minimum in dual and triple coil system, whereas in four coil system out of four split frequency components the lower two are present close to each other, i.e., 7.9 MHz and 8.9 MHz that could cross couple

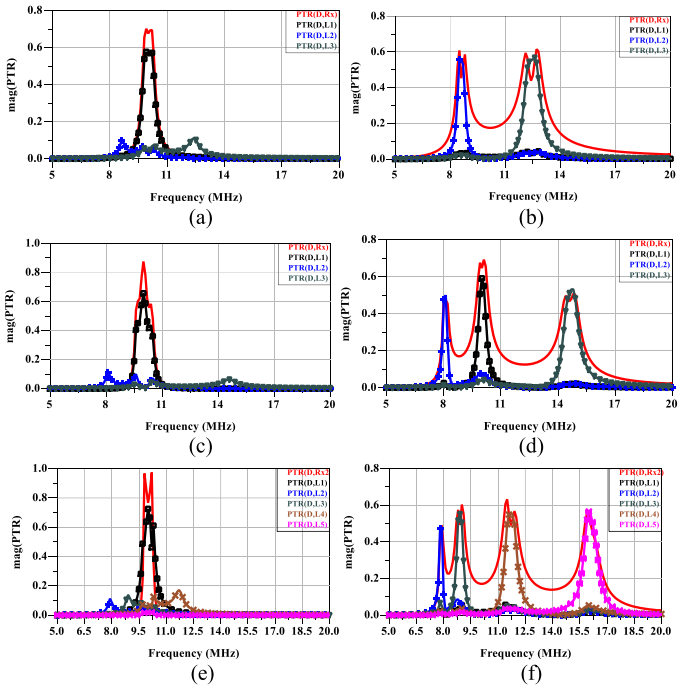

Fig. 7. Magnitude of power transfer ratio for SSWPT system. (a) Dual coil CC mode. (b) Dual coil OC mode. (c) Triple coil CC mode. (d) Triple coil OC mode. (e) Four coil CC mode. (f) Four coil OC mode.

more as compared with other load coils. It can be avoided by placing the closer frequency load coils spaced away from each other in the practical scenario.

C. FEM Modeling and Simulation

The proposed SSWPT systems are modeled and analyzed in Comsol Multiphysics software and the dimensions of the designed coils are the same as given in Table II. The resonant coils are enclosed with a rectangular shape Gaussian boundary. The drive, Tx, Rx coils are designed with multi turn single open conductor type and the load coils are of a lumped port type. The resonant capacitance is connected with the coil terminal and with a load resistance for each load coil. In-built copper material is selected for all the coil with the conductivity of 58.5×10^6 S/m and air is chosen as the surrounding medium. Physics control mesh and frequency domain analysis is selected for meshing and for the study of the designed system. Drive coil is excited with ac source of 10 V, 10 MHz supply with the source resistance of 50 Ω. The magnetic field intensity under CC and OC modes for dual, triple, and four coil SSWPT systems are shown in Fig. 8. The distance between the Tx and Rx coils are changed and analyzed for CC and OC modes of operation. It is observed that in CC mode of operation the load 1, which is designed with the same resonant frequency as of supply frequency is getting much field strength as compared to other coils. When the distance between Tx to Rx is reduced and operated in OC mode, the magnetic field intensity at the other load coils is more, which indicates a uniform distribution of power simultaneously to selected loads. In the dual and four coil SSWPT systems under the OC mode, the load 1 is not getting stronger magnetic field strength as compared with other loads due to change of resonant

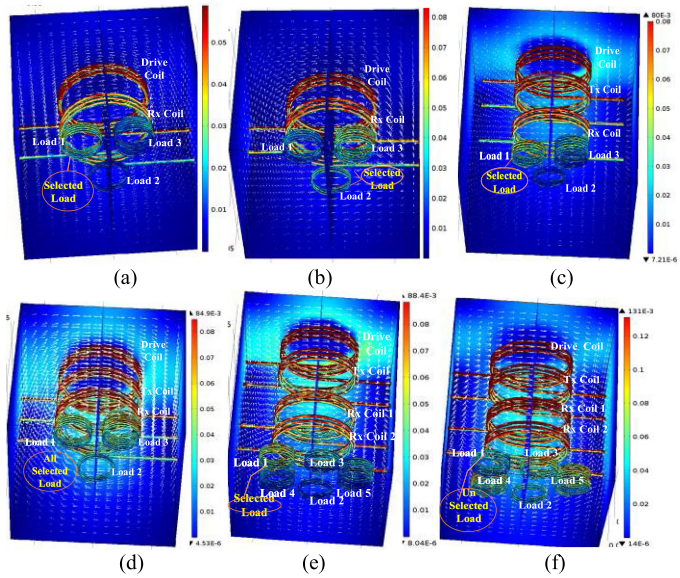

Fig. 8. FEM simulation of SSWPT system. (a) Dual coil CC mode. (b) Dual coil OC mode. (c) Triple coil CC mode. (d) Triple coil OC mode. (e) Four coil CC mode. (f) Four coil OC mode.

TABLE VI
MAGNETIC FIELD INTENSITY ($\times 10^{-3}$) A/M OF SSWPT SYSTEM

Mode	Dual Coil SSWPT			Triple Coil SSWPT			Four Coil SSWPT				
Load	1	2	3	1	2	3	1	2	3	4	5
CC	35-45	8-12	10-15	60-70	8-12	25-38	70-80	8-12	10-15	10-15	15-20
OC	10-15	50-60	55-65	65-75	60-70	65-78	45-52	65-80	105-110	105-110	105-118

frequency in the Rx coil. Whereas in a triple coil SSWPT system, the load 1 is receiving stronger field strength in both the modes of operation. The magnetic field strength values for all the cases under CC and OC modes are presented in Table VI.

D. Automatic Power Flow Control

The load power estimation of SSWPT system can be performed without wireless or wire communication from the load. The output power is determined using the known information of the input voltage (V_D) and current (I_D) alone. Measuring the load power in SSWPT system will be useful to estimate the charging state of the loads and further to increase the number of load coils powered by the same SSWPT system. By changing the position of Tx coil to get another set of frequency split components, and designing the load coils with that frequency, the number of loads can be increased. The position of the Tx coil can be adjusted automatically to the preset value, once the load power reaches to a required value. The schematic diagram of the automatic power flow control method of a dual coil SSWPT system is shown in Fig. 9. The drive coil current, voltage is measured, and the estimation algorithm which runs on a PC or low cost microcontroller determines the load power and changes the position of Tx to a new preset value. However, the change of position will be based on the maximum charging time required by the load in the group. The load power of the proposed system

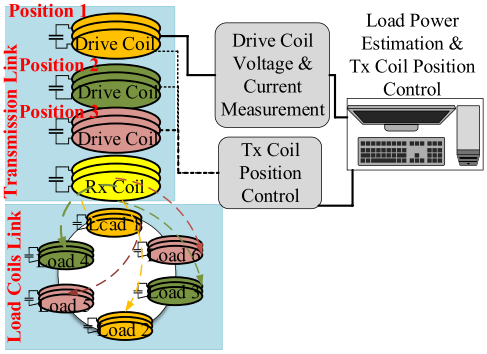

Fig. 9. Automatic power flow control of dual coil SSWPT system.

is derived from the estimated load current in Section III-A. The system parameters such as self-inductance, mutual inductance, resonant frequency, coil resistance, and capacitance values are known parameters and then by measuring V_S and I_D the load currents can be estimated.

The estimated load current from (15)–(17) can be used to determine the load power of the dual coil SSWPT system is

$$P_{L1} = I_{L1}^2 \text{real}\left(Z_{L1}\right)|_{\omega 1}; \quad \text{under CC mode} \tag{24}$$

$$\left.\begin{aligned} P_{L2} &= I_{L2}^2 \text{real}\left(Z_{L2}\right)|_{\omega 2} \\ P_{L3} &= I_{L3}^2 \text{real}\left(Z_{L3}\right)|_{\omega 3} \end{aligned}\right\}; \quad \text{under OC mode.} \tag{25}$$

Similarly, the load power for the triple and four coil SSWPT systems can be derived from (19) to (21) and (22) to (23) as

$$P_{Li} = I_{Li}^2 \text{real}\left(Z_{Li}\right)|_{\omega i}; \quad \left\{\begin{aligned} &i = 1,2,3 \text{ for 3 coil SSWPT} \\ &i = 1..5 \text{ for 4 coil SSWPT} \end{aligned}\right\}. \tag{26}$$

The load current estimation accuracy depends on the measurement accuracy of input voltage, current, circuit parameters $R_i,\ L_i,\ C_i,\ M_{ij}$, and resonant frequency ω. Meanwhile, to increase the accuracy of the estimation, the conduction loss in the coil needs to be reduced which can be obtained by operating the coil with low current and high voltage. The power transfer efficiency of the proposed system to each load is determined as

$$\eta_{DLi} = \frac{P_{Li} - P_{\text{error}}}{P_{\text{in}}}; \quad \left\{\begin{aligned} &i = 1,2,3 \text{ for 2 coil SSWPT} \\ &i = 1,2,3 \text{ for 3 coil SSWPT} \\ &i = 1,2,3 \text{ for 3 coil SSWPT} \end{aligned}\right\} \tag{27}$$

where P_{error} is the estimation error, the load power estimation by this method can be done under fixed load conditions, variation in the load will slightly change the operating frequency of the load, thereby reduction in the efficiency of the system. The simulation of the dual coil SSWPT system with six loads at the coupling coefficients of 0.2, 0.35, and 0.65 are shown in Fig. 10 and the design parameters of load coils are given in Table VII. It is observed that for each case, the corresponding loads designed with the particular resonant frequency are receiving maximum power.

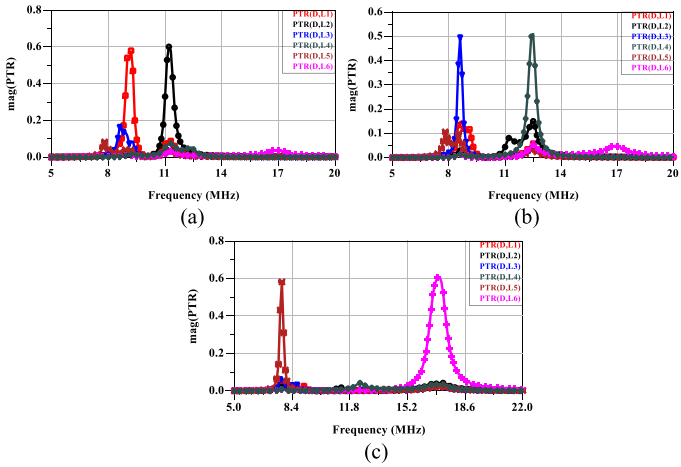

Fig. 10. Dual coil SSWPT PTR -six load. (a) $k = 0.20$. (b) $k = 0.35$. (c) $k = 0.65$.

TABLE VII
DUAL COIL SSWPT PARAMETERS

k	f_1 (MHz)	f_2 (MHz)	L (μH) f_1	L(μH) f_2
0.20	9.1	11.2	30.58	20.19
0.35	8.6	12.4	34.1	16.49
0.65	7.8	16.9	41.6	8.86

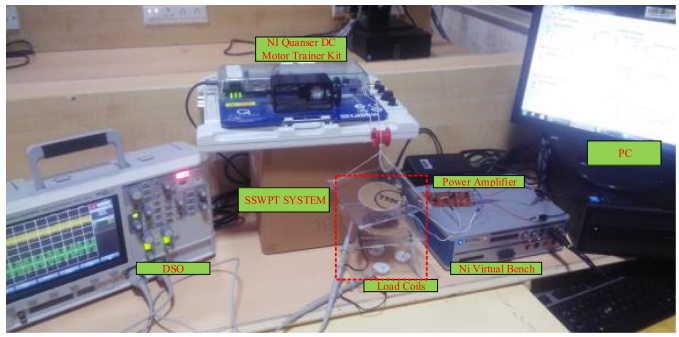

Fig. 11. Experimental setup of SSWPT system.

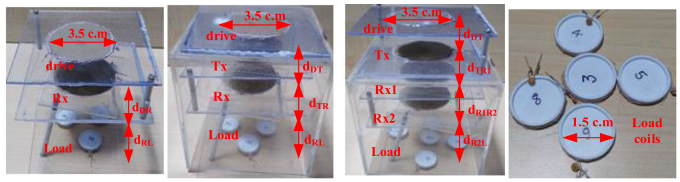

Fig. 12. Measurement coil setup. (a) Dual coil. (b) Triple coil. (c) Four coil. (d) Load coils.

IV. EXPERIMENTAL ANALYSIS

To validate the proposed SSWPT system, an experimental measurement has been conducted and the test setup is shown in Fig. 11. Fig. 12 shows the designed dual, triple, and four transmission link coils and load coils. The drive, Tx, Rx1, Rx2 coils are designed with 28 AWG Litz wire based on the specifications given in Table III and fixed on an acrylic sheet with a piece of cart board in the center for support. The load coils are designed using 32-AWG Litz wire and wound on a round shape

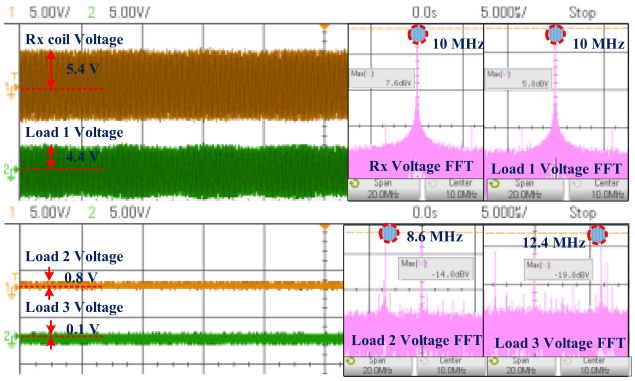

Fig. 13. Dual coil SSWPT system CC mode.

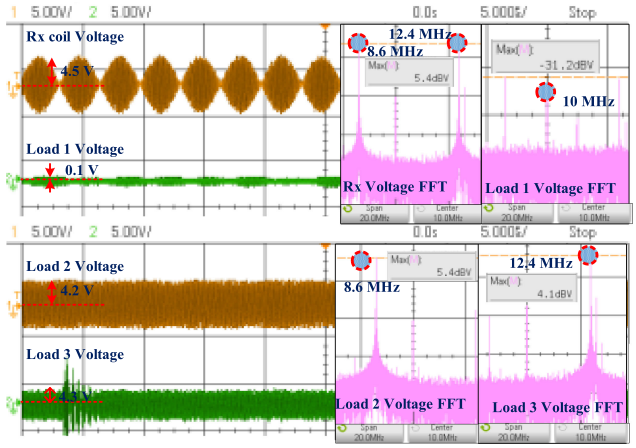

Fig. 14. Dual Coil SSWPT system OC mode.

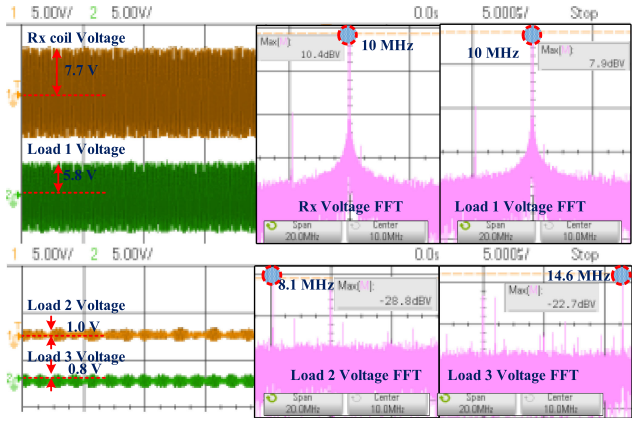

Fig. 15. Triple Coil SSWPT system CC mode.

three-dimensional printed acrylonitrile butadiene styrene plastic material for support. The power source for the drive coil is connected from National Instruments Virtual Bench (NI VB-812) through a power amplifier. The load power estimation algorithm is designed in LabVIEW and for the automatic control of Tx position, NI Quanser dc Motor control setup is utilized due to the readymade availability of the instruments. It has a fine position control mechanism with feedback encoder and data acquisition feature. A spindle is attached with the gear setup to the dc motor to convert the rotational motion into linear displacement. The length of the thread is calibrated based on the angular displacement of dc motor; the developed closed-loop control mechanism automatically adjusts the position of the drive coil. The drive voltage and current are measured using NI VB-812 digital multimeter and the measured data is feed to the developed control algorithm. The position of the dc motor rotor is adjusted based on the estimated load power and the user requirement to change the distance between Tx and Rx. The Rx and load voltages are measured for dual, triple, and four coil SSWPT system using keysight dual channel digital storage oscilloscope.

A. Dual Coil SSWPT

For the dual coil SSWPT system, the drive coil is supplied with 10 V, 10 MHz from the power amplifier and Rx, load voltages are measured under CC and OC mode. Initially the distance between the coil is set to be $d_{DR} = 3.5$ cm in CC mode and the measured voltages are shown in Fig. 13. It is observed that the load 1 voltage of 4.4 V is maximum with the designed resonant frequency of 10 MHz. Fig. 13 also shows the FFT spectrum of measured voltage under CC mode. The distance between the coil is reduced to 2.5 cm to operate in OC mode with the $k_{DR} = 0.35$, the measured Rx voltage has two peaks at 8.6 MHz and 12.4 MHz and the load 1 voltage is minimum. The load 2 and load 3 voltage contains the peaks at 8.6 MHz and 12.4 MHz and the induced voltage of 4.2 V and 4.3 V as shown in Fig. 14. It is seen that under the OC mode, the Rx coil consist of two frequency components which are divided and evenly transferred to the harmoniously tuned load 2 and load 3 coils. The magnitude of the cross coupling voltage in each load is very less as compared with individual load resonant voltage. The distance between Rx and load coils is fixed at 3.5 cm in such a way that it will not make OC with Rx coil irrespective modes of operation.

B. Triple Coil SSWPT

The distance between the drive and Tx coils are fixed to 2 cm with $k_{DT} = 0.4$ and the distance between Tx to Rx is set to be 3.5 cm for CC mode. The load 1 is receiving the rms voltage of 5.8 V at 10 MHz, and load 2 and load 3 voltages are less than 0.2 V as shown in Fig. 15. When d_{TR} changed to 2.5 cm with the coupling of $k_{TR} = 0.35$, the Rx voltage peaks are present in three different frequencies of 8.1 MHz, 10 MHz, 14.6 MHz with the rms voltage of 5.9 V, 3.8 V, and 4.1 V, respectively, as shown in Fig. 16. The cross coupling effects are still present at each load voltage, but the magnitude of cross coupling voltage is less than 0.1 V which is in the permissible range. It is noticed that in the triple coil system, the source resonant frequency also existing along with the bifurcation frequency, whereas, in a dual coil system, the resonant frequency of the source is diminished. Similar to the dual coil system, the distance between the load and Rx coil is maintained at 3.5 cm in both the modes of operation. In OC mode due to frequency bifurcation present in the transmission side, the Rx voltage is not appearing as a single sinusoidal waveform due to multiple frequencies. At the same time, the loads which are in resonant with the split frequencies

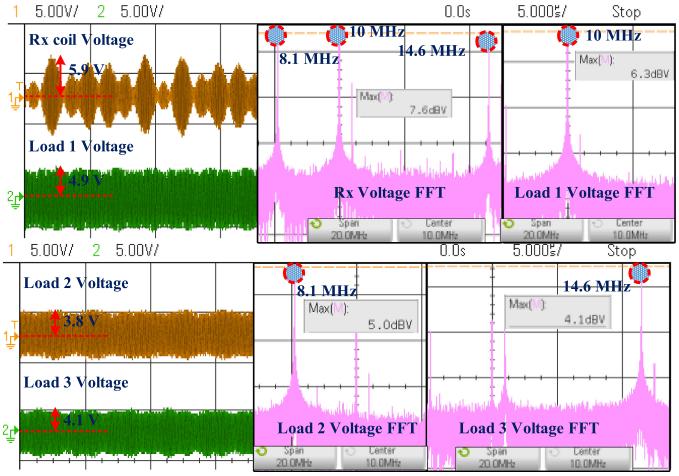

Fig. 16. Triple Coil SSWPT system OC mode.

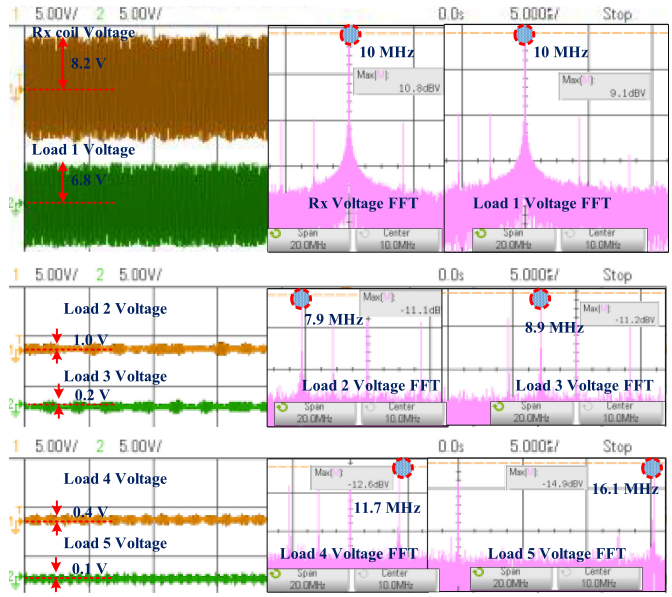

Fig. 17. Four Coil SSWPT system CC mode.

are getting maximum induced voltage and maintaining the sinusoidal nature of the waveform. The non-sinusoidal nature of the waveform is because of multiple frequencies in the Rx coil and the non-resonance condition of the load coils. The triple coil system could be useful in applications such as master slave swarm robot control, where the master robot always requires power to operate and to make a decision.

C. Four Coil SSWPT

For the four coil SSWPT, the d_{DT} and d_{R1R2} are fixed to be 2 cm with the coupling of $k_{DT} = k_{R1R2} = 0.4$ and the d_{TR1} are changed for CC and OC mode. Under the CC mode the d_{TR1} is set to 3.5 cm and the voltages across Rx2, load are measured as shown in Fig. 17. The peak value Rx2 voltage occurs at 10 MHz and the load 1 voltage is 6.8 V. As the system is operated in OC mode by changing d_{TR1} and the coupling k_{TR1} to be 0.35, Rx2 contains four peak voltages at 7.9 MHz, 8.9 MHz, 11.6 MHz, and 16.1 MHz as shown in Fig. 18. The load 1 to load 5

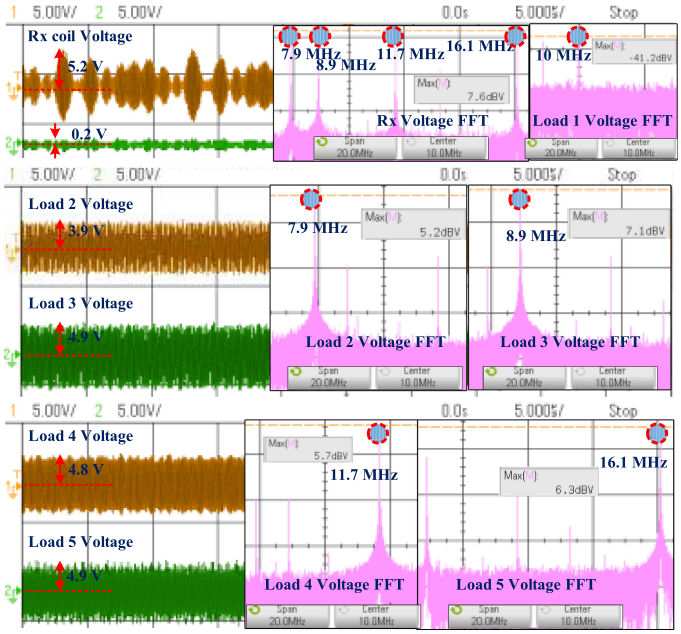

Fig. 18. Four Coil SSWPT system OC mode.

TABLE VIII
RMS VOLTAGE OF DUAL COIL SSWPT

V_{RMS}(V)	Mode	f_1=10	f_2=8.6	f_3=12.4
V_{RX}	CC	5.4	0.01	0.01
	OC	0.3	4.4	4.5
V_{L1}	CC	4.4	0.01	0.01
	OC	0.1	0.2	0.2
V_{L2}	CC	0.8	1.1	0.01
	OC	0.1	4.2	0.4
V_{L3}	CC	0.1	0.2	0.4
	OC	0.41	0.1	4.3

TABLE IX
RMS VOLTAGE OF TRIPLE COIL SSWPT

V_{RMS}(V)	Mode	f_1=10	f_2=8.1	f_3=14.6
V_{RX}	CC	7.7	0.01	0.01
	OC	5.9	3.8	4.1
V_{L1}	CC	5.8	0.01	0.01
	OC	4.9	0.1	0.2
V_{L2}	CC	0.01	1.0	0.01
	OC	0.8	3.8	0.2
V_{L3}	CC	0.01	0.01	0.8
	OC	0.4	0.01	4.1

voltages at OC mode are 0.2 V, 3.9 V, 4.9 V, 4.8 V, and 4.9 V, respectively. Since the load 1 is not in resonance with the Rx2 under OC mode the induced voltage is very less and the load 2 to load 5 voltages are maximum due to the OC resonance with the Rx2 coil. The experimental results of rms value of voltage across the Rx and load coils of dual, triple, and four coil SSWPT systems are given from Tables VIII-X.

TABLE X
RMS VOLTAGE OF FOUR COIL SSWPT

V_{RMS}(V)	Mode	f_1=10	f_2=7.9	f_3=8.9	f_4=11.7	f_5=16.1
V_{RX}	CC	8.2	0.01	0.01	0.01	0.01
	OC	0.6	3.9	5.0	5.2	4.9
V_{L1}	CC	6.8	0.01	0.01	0.01	0.01
	OC	0.2	0.1	0.1	0.1	0.1
V_{L2}	CC	0.1	1.0	0.1	0.1	0.1
	OC	0.1	3.9	0.8	0.2	0.2
V_{L3}	CC	0.1	0.1	1.0	0.01	0.01
	OC	0.01	1.0	4.9	0.8	0.2
V_{L4}	CC	0.2	0.01	0.01	0.4	0.01
	OC	0.4	0.4	0.2	4.8	0.8
V_{L5}	CC	0.1	0.01	0.01	0.01	0.01
	OC	0.01	0.01	0.01	0.6	4.9

TABLE XI
DUAL COIL SSWPT SYSTEM AT DIFFERENT k_{DR}

V_{RMS} (V) \ f (MHz)	Position 1		Position 2		Position 3	
	9.1	11.2	8.6	12.4	7.8	16.9
V_{RX2}	4.3	4.4	4.1	4.2	4.3	4.4
V_{L1}	3.9	0.02	0.4	0.02	0.2	0.02
V_{L2}	0.03	3.8	0.05	0.5	0.02	0.4
V_{L3}	0.2	0.01	3.85	0.7	0.01	0.4
V_{L4}	0.02	0.1	0.2	3.76	0.2	0.02
V_{L5}	0.2	0.04	0.1	0.4	3.9	0.1
V_{L6}	0.01	0.2	0.01	0.6	0.02	3.7

D. Automatic Power Flow Control

Based on the design parameters and the load power requirement the desired position of the Tx coil will be adjusted with the automatic power flow control algorithm to charge the different set of loads.

By selecting the coil system (dual/ triple/ four) and entering the impedance matrix, load resistance values of the output power will be estimated. The power flow control method is tested for the dual coil SSWPT system with an additional four load coils. Initially, the distance between the drive and source coil is set to be 1.0 cm to get $k_{DR} = 0.65$ and the load voltages are measured. The maximum voltages of 1.9 V and 1.7 V are received in load 5 and load 6 at the frequency of 7.8 MHz and 16.9 MHz, respectively. Next d_{DR} is set to 2 cm with the $k_{DR} = 0.35$ and the maximum voltages of 1.85 V and 1.76 V occurs at load 3 and load 4, respectively. Finally, the d_{DR} is increased to 2.8 cm with $k_{DR} = 0.2$, the load 1 and load 2 are receiving maximum voltages of 1.9 V, 1.8 V at 9.1 MHz, 11.2 MHz, respectively. The measured load voltages of the dual coil SSWPT system at different coupling are given in Table XI.

The efficiency of the proposed system is calculated from the maximum value of the load voltage in the group with drive coil voltage at fixed load condition. Table XII gives a comparative analysis of different power transfer methods for multiple load

TABLE XII
COMPARISON OF POWER TRANSFER EFFICIENCY IN MULTIPLE RECEIVER MRWPT SYSTEM

Method	Distance Rx Load (c.m)	Max number of Loads	Extra Control	Power Division	Efficiency %	Coupling Sensitivity	Remarks
[8]	28	2	Yes	No	60	Yes	Suitable for static environment
[17]	13	2	Yes	No	55	No	Applicable to dynamic condition
[18]	4.2	3	Yes	Yes	29	No	Applicable to dynamic condition
This Work	3.5	2,3,4	No	Yes	33, 46, 67	Yes	Load coils can be dynamic but the Tx section coils is static

system with the proposed system. It is observed that the proposed system does not requires any extra control circuitry to change the frequency and power flow between the drive and load. The reduction in the number of coil is possible by pacing the intermediate coils at a different angle with respect to source coil and operating it at over coupling mode, thereby the triple coil WPT system can function as four coil WPT. The comparison of the proposed method with the literature is given in Table XII.

V. CONCLUSION

This paper has demonstrated the frequency bifurcation based SSWPT system to multiple load coil. The SSWPT system can provide a uniform power distribution to multiple resonant loads with negligible cross coupling in a proximate environment. The theoretical, simulation, and experimental results validate the proposed dual, triple, and four coil SSWPT systems suitable for simultaneously charging two, three, and four loads, respectively. The results confirming the proposed power transfer strategy to attain the higher power transfer efficiency of 39.34%, 49.31%, and 68.22% with a negligible cross coupling of -31.2 dBV, -36.2 dBV, and -41.2 dBV for dual, triple, and four coil, respectively. In addition, the implementation of automatic power flow control for the dual coil SSWPT increases the number of loads to six at the different coupling point. The proposed method can be employed in the simultaneous power transfer applications such as distributed implants, wireless sensor networks, and micro robot.

REFERENCES

[1] S. Y. R.Hui, W. Zhong, and C. K. Lee, "A critical review of recent progress in mid-range wireless power transfer," *IEEE Trans. Power Electron.*, vol. 29, no. 9, pp. 4500–4511, Sep. 2014.
[2] Y. M. Roshan and E. J. Park, "Design approach for a wireless power transfer system for wristband wearable devices," *IET Power Electron.*, vol. 10, no. 8, pp. 931–937, Jun. 2017.
[3] A. Daga, J. M. Miller, B. R. Long, R. Kacergis, P. Schrafel, and J. Wolgemuth, "Electric fuel pumps for wireless power transfer: Enabling rapid growth in the electric vehicle market," *IEEE Power Electron. Mag.*, vol. 4, no. 2, pp. 24–35, Jun. 2017.
[4] B. Deng, S. Li, B. Li, J. Wang, and Z. Zhang, "Noninvasive brain stimulation using strong-coupling effect of resonant magnetics," *IEEE Trans. Magn.*, vol. 53, no. 5, pp. 1–9, May 2017.

[5] R. Johari, J. V. Krogmeier, and D. J. Love, "Analysis and practical considerations in implementing multiple transmitters for wireless power transfer via coupled magnetic resonance," *IEEE Trans. Indus. Electron.*, vol. 61, no. 4, pp. 1774–1783, Apr. 2014.
[6] J. Kim, H. C. Son, D. H. Kim, and Y. J. Park, "Impedance matching considering cross coupling for wireless power transfer to multiple receivers," in *Proc. IEEE Wireless Power Transf.*, 2013, pp. 226–229.
[7] Z. Pantic, K. Lee, and S. M. Lukic, "Receivers for multifrequency wireless power transfer: Design for minimum interference," *IEEE J. Emerg. Sel. Topics Power Electron.*, vol. 3, no. 1, pp. 234–241, Mar. 2015.
[8] C. K. Lee, W. X. Zhong, and S. Y. R. Hui, "Effects of magnetic coupling of nonadjacent resonators on wireless power domino-resonator systems," *IEEE Trans. Power Electron.*, vol. 27, no. 4, pp. 1905–1916, Apr. 2012.
[9] M. Haerinia and E. S. Afjei, "Investigation of receiving pot core effect on magnetic flux density in inductive coupling-based wireless power transfer," in *Proc. Int. Symp. Power Electron., Elect. Drives, Autom. Motion*, 2016, pp. 541–545.
[10] A. K. Ramrakhyani and G. Lazzi, "Interference-free wireless power transfer system for biomedical implants using multi-coil approach," *Electron. Lett.*, vol. 50, no. 12, pp. 853–855, Jun. 5, 2014.
[11] R. Das and H. Yoo, "A multiband antenna associating wireless monitoring and nonleaky wireless power transfer system for biomedical implants," *IEEE Trans. Microw. Theory Techn.*, vol. 65, no. 7, pp. 2485–2495, Jul. 2017.
[12] B. L. Cannon, J. F. Hoburg, D. D. Stancil, and S. C. Goldstein, "Magnetic resonant coupling as a potential means for wireless power transfer to multiple small receivers," *IEEE Trans. Power Electron.*, vol. 24, no. 7, pp. 1819–1825, Jul. 2009.
[13] J. Kim, D. H. Kim, and Y. J. Park, "Analysis of capacitive impedance matching networks for simultaneous wireless power transfer to multiple devices," *IEEE Trans. Ind. Electron.*, vol. 62, no. 5, pp. 2807–2813, May 2015.
[14] J. Kim, D. H. Kim, and Y. J. Park, "Free-positioning wireless power transfer to multiple devices using a planar transmitting coil and switchable impedance matching networks," *IEEE Trans. Microw. Theory Techn.*, vol. 64, no. 11, pp. 3714–3722, Nov. 2016.
[15] M. Fu, T. Zhang, X. Zhu, P. C. K. Luk, and C. Ma, "Compensation of cross coupling in multiple-receiver wireless power transfer systems," *IEEE Trans. Ind. Informat.*, vol. 12, no. 2, pp. 474–482, Apr. 2016.
[16] W. Zhong and S. Y. R. Hui, "Auxiliary circuits for power flow control in multifrequency wireless power transfer systems with multiple receivers," *IEEE Trans. Power Electron.*, vol. 30, no. 10, pp. 5902–5910, Oct. 2015.
[17] Y. Zhang, T. Lu, Z. Zhao, F. He, K. Chen, and L. Yuan, "Selective wireless power transfer to multiple loads using receivers of different resonant frequencies," *IEEE Trans. Power Electron.*, vol. 30, no. 11, pp. 6001–6005, Nov. 2015.
[18] Y. J. Kim, D. Ha, W. J. Chappell, and P. P. Irazoqui, "Selective wireless power transfer for smart power distribution in a miniature-sized multiple-receiver system," *IEEE Trans. Ind. Electron.*, vol. 63, no. 3, pp. 1853–1862, Mar. 2016.
[19] L. Tan, J. Guo, X. Huang, and F. Wen, "Output power stabilisation of wireless power transfer system with multiple transmitters," *IET Power Electron.*, vol. 9, no. 7, pp. 1374–1380, Jun. 8, 2016.
[20] K. Lee and D. H. Cho, "Diversity analysis of multiple transmitters in wireless power transfer system," *IEEE Trans. Mag.*, vol. 49, no. 6, pp. 2946–2952, Jun. 2013.
[21] Y. Zhang, T. Lu, Z. Zhao, K. Chen, F. He, and L. Yuan, "Wireless power transfer to multiple loads over various distances using relay resonators," *IEEE Microw. Wireless Compon. Lett.*, vol. 25, no. 5, pp. 337–339, May 2015.
[22] T. Nguyen, S. H. Kang, J. H. Choi, and C. W. Jung, "Magnetic resonance wireless power transfer using three-coil system with single planar receiver for laptop applications," *IEEE Trans. Consum. Electron.*, vol. 61, no. 2, pp. 160–166, May 2015.
[23] Y. Zhang, Z. Zhao, and T. Lu, "Quantitative analysis of system efficiency and output power of four-coil resonant wireless power transfer," *IEEE J. Emerg. Sel. Topics Power Electron.*, vol. 3, no. 1, pp. 184–190, Mar. 2015.
[24] S. Moon and G. W. Moon, "Wireless power transfer system with an asymmetric four-coil resonator for electric vehicle battery chargers," *IEEE Trans. Power Electron.*, vol. 31, no. 10, pp. 6844–6854, Oct. 2016.
[25] R. Huang, B. Zhang, D. Qiu, and Y. Zhang, "Frequency splitting phenomena of magnetic resonant coupling wireless power transfer," *IEEE Trans. Mag.*, vol. 50, no. 11, pp. 1–4, Nov. 2014.
[26] W. Niu, W. Gu, J. Chu, and A. Shen, "Frequency splitting patterns in wireless power relay transfer," *IET Circuits, Dev. Syst.*, vol. 8, no. 6, pp. 561–567, Nov. 2014.
[27] H. Nguyen and J. I. Agbinya, "Splitting frequency diversity in wireless power transmission," *IEEE Trans. Power Electron.*, vol. 30, no. 11, pp. 6088–6096, Nov. 2015.
[28] S. Huang, Z. Li, and K. Lu, "Frequency splitting suppression method for four-coil wireless power transfer system," *IET Power Electron.*, vol. 9, no. 15, pp. 2859–2864, Dec. 14, 2016.
[29] Y. L. Lyu *et al.*, "A method of using nonidentical resonant coils for frequency splitting elimination in wireless power transfer," *IEEE Trans. Power Electron.*, vol. 30, no. 11, pp. 6097–6107, Nov. 2015.
[30] W. Choi, C. Park, and K. Lee, "Circuit analysis of achievable transmission efficiency in an overcoupled region for wireless power transfer systems," *IEEE Syst. J.*, vol. 12, no. 4, pp. 3873–3876, Dec. 2018.
[31] H. Lee, K. Lee, H. Kim, and I. Lee, "Wireless information and power exchange for energy-constrained device-to-device communications," *IEEE Internet Things J.*, vol. 5, no. 4, pp. 3175–3185, Aug. 2018.
[32] H. Wheeler, "Simple inductance formulas for radio coils," *Proc. Inst. Radio Eng.*, vol. 16, no. 10, pp. 1398–1400, Oct. 1928.

Narayanamoorthi R. (M'18) received the bachelor's degree in electrical engineering and the master's degree in control and instrumentation from Anna University, Chennai, India, in 2009 and 2011 respectively, and the Doctoral degree from the SRM Institute of Science and Technology, Chennai, India, in 2019.

From 2012 onwards, he is serving as an Assistant Professor at SRM Institute of Science and Technology. His research interests include wireless power transfer, biomedical sensor, gas sensors, solar PV, fuel cell, and smart sensor materials.

Vimala Juliet A. received the B.E. degree from Bharathiar University, Coimbatore, India, in 1992, and the M.E. and Ph.D. degrees from Anna University, Chennai, India, in 1994 and 2005, respectively, all in electronics and instrumentation engineering.

Since 1995, she has been with the Department of Electronics and Instrumentation Engineering, SRM Institute of Science and Technology, Kattankulathur, India, where she is currently a Professor and the Head of the department.

Bharatiraja Chokkalingam (M'11) received the B.E. degree in electrical and electronics engineering from the Kumaraguru College of Engineering, Coimbatore, India, in 2002, the M.E. degree in power electronics engineering from the Government College of Technology, Coimbatore, India, in 2006, and the Ph.D. degree in electrical engineering from SRM University, Chennai, India, in 2015.

He completed the Postdoctoral Fellowship with the Department of Electrical and Computer Engineering, Northeastern University, Boston, MA, USA, and Centre for Energy and Electric Power, Tshwane University of Technology, Pretoria, South Africa, in 2018 and 2016, respectively. He is currently working as an Associate Professor with the Department of Electrical and Electronics Engineering, SRM Institute of Science and Technology. His research interest includes power electronic converters, inverters and drives, electrical vehicle, wireless power transfer and smart grid.

Dr. Chokkalingam was the recipient of prestigious award Bhaskara Advanced Solar Energy, DST Govt. of India and IUSSTF at 2017.